



# Evaluation of Seismic Deflection Amplification Factor for Buildings Utilizing Cold-Formed Steel–Framed Shear Walls

Mohammed M. Eladly<sup>1</sup> and Benjamin W. Schafer, A.M.ASCE<sup>2</sup>

**Abstract:** The seismic deflection amplification factor for a series of archetype buildings utilizing cold-formed steel–framed shear walls was investigated. A total of 118 archetype buildings were considered, of which 83 employed cold-formed steel–framed shear walls with steel sheathing, and 35 employed wood structural panel sheathing. Using nonlinear equivalent single-degree-of-freedom (SDOF) models, nonlinear time-history analyses for the 118 archetype buildings subjected to the 44 FEMA P-695 earthquakes were conducted. In these SDOF models, the actual response of shear walls obtained from experimental studies was used to define the nonlinear material parameters. The AISI S400 deflection expression was evaluated using experimental data, and numerically predicted deflection amplification factors were calculated and compared against that recommended in current practice. The results show that current practice may overestimate expected deflections. To address this issue, and to simplify design, a linearization of the AISI S400 deflection expression is recommended. With appropriate choice of the force level, the linearized AISI S400 deflection expression leads to acceptable drift predictions with the currently employed deflection amplification factor. **DOI: 10.1061/JSENDH.STENG-11987.** © 2023 American Society of Civil Engineers.

Author keywords: Earthquake engineering; Deflection amplification factor; Cold-formed steel; Shear walls; Numerical modeling.

### Introduction

Current seismic design, utilizing equivalent lateral force and linear structural models, considerably decreases design level seismic forces to exploit the system level overstrength and earthquake energy dissipation capacity of complete buildings. This concept is illustrated in Fig. 1, which shows a typical base shear (V) versus lateral drift  $(\delta)$  relation envelope. The level of design seismic forces required if the response of the considered structure is within the elastic range is represented by the force demand at Point A in Fig. 1  $(V_e)$ . For strength design, this elastic force level is decreased, using a seismic response modification coefficient for forces (R), to the level of Point B  $(V_r)$ .

To calculate the maximum inelastic drift  $\delta^{\text{peak}}$  (Fig. 1, Point C) that may be reached in a seismic design earthquake event, the elastic design displacement is amplified by a deflection amplification factor,  $C_d$ 

$$\delta^{\text{peak}} = C_d \delta_r^e \tag{1}$$

Implicit in Eq. (1) for application in ASCE 7 (ASCE 2022) is the assumption that we have assumed Risk Category I or II and  $I_e = 1.0$  for the work reported herein.

For seismic design, drift often is more important than strength when damage and even collapse are much more tightly connected with drift than strength levels, and thus it is important to determine  $\delta^{\text{peak}}$ : (1) determine maximum story drifts; (2) verify deformation capacity of critical elements in the structure; (3) evaluate *P*-delta effects; and (4) calculate minimum structure separation to avoid pounding.

Numerous studies have investigated the deflection amplification factor for building structures. Uang and Maarouf (1994) performed an analytical investigation of the dynamic performance of four instrumented buildings and recommended increasing the deflection amplification factor to at least the seismic response modification coefficient for forces (R) to calculate peak drifts. Kurban and Topkaya (2009) numerically evaluated response modification (R), overstrength  $(\Omega_o)$ , and displacement amplification  $(C_d)$  factors for steel plate shear wall (SPSW) systems, and, depending on the generated numerical data, they developed equations relating R to  $C_d$ . To assess the ratio of the  $C_d$  to R for RC frames, an analytical study of the seismic responses of these frames to a suite of earthquake records was conducted by Samimifar et al. (2015). Based on the study findings, it was recommended that the  $C_d/R$  ratio should be equal to or greater than 1.0 to determine inelastic drifts. Kuşyılmaz and Topkaya (2016) conducted a numerical study to assess seismic response factors for a different type of frame [steel eccentrically braced frames (EBFs)]. Six archetypes were investigated, and the FEMA P = 695 (FEMA 2009) methodology was employed in the study. The findings showed that designs based on the response factors in the US specifications (at the time of the study) had higher collapse probabilities than expected. Mohammadi and Kordbagh (2018) explored the impact of panel zone on the story drift and  $C_d$ . Four-story steel moment frames with different thicknesses of the panel zone were investigated using nonlinear time-history analysis. The results showed that the panel zone should be taken into consideration when modeling; otherwise, the story drift could be underestimated by as much as 35%.

Several researchers have investigated the effect of building height on  $C_d$  and other seismic response modification coefficients. Hsiao et al. (2013) performed nonlinear dynamic analyses of a

<sup>&</sup>lt;sup>1</sup>Graduate Research Assistant, Dept. of Civil and Systems Engineering, Johns Hopkins Univ., Baltimore, MD 21218 (corresponding author). ORCID: https://orcid.org/0000-0001-7951-620X. Email: eladly@jhu.edu; eladly@ymail.com

<sup>&</sup>lt;sup>2</sup>Hackerman Professor, Dept. of Civil and Systems Engineering, Johns Hopkins Univ., Baltimore, MD 21218. Email: schafer@jhu.edu

Note. This manuscript was submitted on August 17, 2022; approved on February 14, 2023; published online on April 21, 2023. Discussion period open until September 21, 2023; separate discussions must be submitted for individual papers. This paper is part of the *Journal of Structural Engineering*, © ASCE, ISSN 0733-9445.

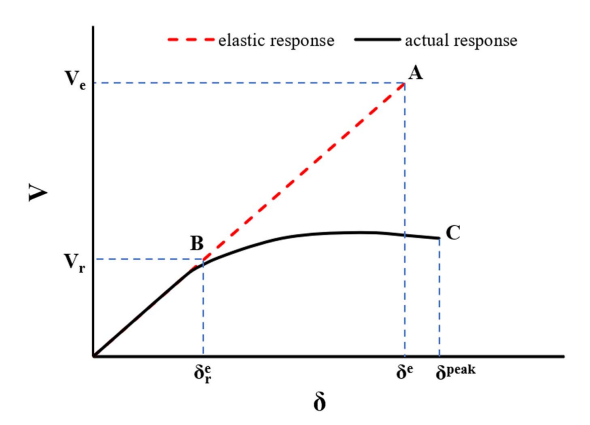


Fig. 1. General structural response.

series of 3-, 9-, and 20-story special concentrically braced frames (SCBFs) to evaluate  $C_d$ , R, and  $\Omega_o$ . Based on their results, they concluded that to realize a consistent margin of safety against collapse, a significantly lower R factor is required for low-rise SCBFs (3-story), whereas midrise and high-rise SCBFs (9- and 20-story) may continue to employ the current R value. Seker et al. (2014) performed nonlinear dynamic time-history and pushover analyses of 4-, 9-, and 20-story steel moment-resisting frames (SMRFs) to assess the influence of building height on  $C_d$  for such structures. The results indicated that the practice at the time of study for finding the inelastic story drifts for SMRFs was rational and the frames designed complying with the code requirements could sustain the plastic deformations resulting from design earthquakes when seismically designed and detailed. To verify the effectiveness of R,  $\Omega_o$ , and  $C_d$ , 20 special and 20 ordinary RC walls (archetypes), with different seismic design conditions and physical properties were considered by Gogus and Wallace (2015). Their results demonstrated that the parameters of the archetypes designed based on code provisions were within acceptable limits, with the exception of archetypes with height-to-length aspect ratios of 3 or greater, for which the use of a larger R values is suggested.

Some studies have suggested analytical methods for calculating  $C_d$  (or directly calculating the maximum lateral inelastic deflection) for different steel systems. Fahnestock et al. (2007) proposed a method to determine the peak lateral nonlinear displacement of buckling-restrained braced frames (BRBFs). The method delivered more-accurate predictions for plastic deflections (with a discrepancy of 7%) than AISC predictions, which had a discrepancy of 16%. Another study of BRBFs, by Yakhchalian et al. (2020), formulated analytical expressions to determine  $C_d$  at different story levels, taking into account the number of stories, the fundamental period of the structure, and the strain-hardening ratio. To minimize the differences between the mean values of  $C_d$  calculated numerically and that predicted by their suggested expressions, a random search algorithm was employed, delivering an average deviation of 5% from numerical results. A similar study, but fn eccentrically braced frames (EBFs), by Kuşyılmaz and Topkaya (2015) developed an expression for determining  $C_d$  at different story levels. This expression was able to provide predictions with an average discrepancy of less than 8% compared with numerical data. The accuracy of the aforementioned methods for determining  $C_d$  was determined based on the mean results obtained from nonlinear analyses of systems under design-basis earthquakes (DBEs).

All these efforts helped to assess the deflection amplification factor,  $C_d$ , for different structural systems, and offered enhanced understanding of issues that impact  $C_d$ . To date, there is no

exhaustive research study investigating  $C_d$  for structures utilizing cold-formed steel (CFS) shear walls. Therefore this paper presents an extensive numerical study of the deflection amplification factor for a set of archetype buildings employing cold-formed steel shear walls. Firstly, nonlinear single-degree-of-freedom (SDOF) models were constructed in OpenSees version 3.0.3 to represent the behavior of archetype buildings with CFS shear walls. Then, employing these models, nonlinear time-history analyses for 118 different archetype buildings, utilizing either steel sheet (SS) or wood structural panel (WSP) CFS shear walls, were conducted. Each of the 118 archetype buildings was excited by the 44 different FEMA P-695 earthquakes at the design level, and hence a total of 5,192 cases (118 building  $\times$  44 EQs) were taken into account. Subsequently, the AISI S400 (AISI 2020) deflection equation was assessed depending on results from 35 WSP and 83 SS cold-formed steel shear walls tested. Finally, using the results of the numerical analyses of the 5,192 cases, four different methods for determining deflection amplification factors (including experimental-based, current-practice, and two suggested methods) were examined and compared.

### **Current US Specifications for Seismic Design**

Seismic equivalent lateral force (ELF)-based design per ASCE 7 (ASCE 2022) adopts the approach explained in the section "Introduction" for calculating the required shear demand and the expected peak drift in the seismic event, where

$$V_r = \frac{V_e}{R} \tag{2}$$

where  $V_r$  = required shear demand;  $V_e$  = predicted elastic shear demand; and R = seismic response modification coefficient for force provided in ASCE 7. The seismic response modification coefficient has two primary sources, and may be understood as

$$R = R_{\mu}R_{o} \quad \text{or} \quad \cong R_{\mu}\Omega_{o}$$
 (3)

where  $R_{\mu}$  = modification due to inelasticity or ductility; and  $R_o$  = modification due to overstrength, and an upper-bound approximation of  $R_o$  is the overstrength factor of ASCE 7-22,  $\Omega_o$  (ATC 1995).

The expected maximum drift in a seismic event,  $\delta^{\text{peak}}$ , may be expressed as

$$\delta^{\text{peak}} = C_d \delta^e(V_r) \tag{4}$$

where  $C_d$  = deflection amplification factor;  $\delta^e$  = elastic drift; and  $\delta^e(V_r)$  indicates that the elastic drift is taken at the force level  $V_r$ , and in practice is a static drift from the ELF demands.

According to ASCE 7-22, for "light-frame (cold-formed steel) walls sheathed with wood structural panels rated for shear resistance or steel sheets,"  $R=6.5,~\Omega_o=3,~{\rm and}~C_d=4.$ 

In current cold-formed steel design practice,  $\delta^e(V_r)$  is determined from AISI S400-20 based on the seismic force resisting system (SFRS). For wood structural panel—sheathed shear walls and steel sheet (SS)-sheathed shear walls, the expression takes the following form:

$$\delta^{e} = \frac{2vh^{3}}{3EA_{c}b} + \omega_{1}\omega_{2}\frac{vh}{\rho Gt_{\text{sheathing}}} + \omega_{1}^{5/4}\omega_{2}\omega_{3}\omega_{4}\left(\frac{v}{\beta}\right)^{2} + \frac{h}{b}\delta_{v} \quad (5)$$

where all variables are defined in AISI S400-20; these definitions are provided in the Appendix to this paper. The first term in the equation addresses the chords' deformation, the second term accounts for shear in the sheathing material, the third or nonlinear

term is derived empirically from testing, and the final term provides the contribution from hold-downs or other interstory connections. The demand V is modified to per unit length by dividing by the wall length b, i.e., v = V/b, and the coefficients for WSP and SS shear walls are different, but the form of the expression remains the same (see Appendix). Furthermore, in this paper,  $\delta_{S400}$  is used to refer to the deflection calculated by Eq. (5).

The AISI S400 deflection expression [Eq. (5)] was fit to onesided shear walls (i.e., the nonlinear term in the deflection expression was fit to direct testing on one-sided shear walls). However, AISI S400 allows for the use of 2 times the AISI S400 tables' capacity in the case of two-sided shear walls.

All SFRS respond nonlinearly to force; this is the essence of the  $R_\mu$  force reduction in ELF design. However, the prototypical ductile system is one in which the response is elastic-plastic. Therefore

$$\delta^e(V_r) = V_r/k^e \tag{6}$$

where  $k^e$  = elastic stiffness of the system. In this scenario, expected seismic drift is

$$\delta = C_d V_r / k^e \tag{7}$$

Current CFS practice uses a  $\delta^e(V_r)$  that is nonlinear [Eq. (5)], and hence there is some mixing of the ductile response amplification attributed to  $C_d$  and that embedded in Eq. (5). In addition, the use of a nonlinear deflection expression complicates design. The stiffness of the shear walls is needed to determine how much of the lateral force the shear walls take, and the stiffness of the shear walls is itself a function of the force they take. This requires iteration (i.e., several cycles of redesign), e.g., the CFS-Network for Earthquake Engineering Simulation (NEES) building design demonstrates what this looks like for a practicing engineer (Madsen et al. 2011).

This paper hypothesized that the expected peak deflection  $[\delta^{\mathrm{peak}} = C_d \delta^e(V_r)]$  may be greater than the actual deflection (i.e., the post-peak-strength deflection corresponding to 80% of the peak strength) due to current procedures (AISI S400 and ASCE 7-22). To this end, the application of the deflection expression in AISI S400 and the  $C_d$  recommended in ASCE 7-22 were assessed in this study.

#### Methods

This study numerically investigated archetype buildings employing cold-formed steel–framed shear walls. Two basic rectangular building floor plans were considered, one with a relatively large plan area [48 × 116 ft (14.63 × 35.36 m)] and with a total weight of 240,000 lbf/floor (1,068 kN/floor), and a second with a relatively small plan area [24 × 50 ft (7.3 × 15.24 m)] and with a total weight of 40,000 lbf/floor (178 kN/floor). The per floor weight calculations were based on the data of professionally designed CFS buildings for seismic testing: CFS-NEES for the small building (Schafer et al. 2016), and CFS-Natural Hazards Engineering Research Infrastructure (NHERI) for the large building (Singh et al. 2022). Plan views of the small and large archetype buildings highlighting shear walls' locations are provided in Fig. 2. The shear wall numbers and locations in Fig. 2 are not typical for all studied cases; details are provided in Table 3.

According to ASCE 7-22, the approximate fundamental period  $(T_b)$  for a CFS building can be calculated using Eq. (8), where H is the building height in feet and  $T_b$  is in seconds

$$T_b = 0.02H^{0.75} \tag{8}$$

The estimated period ( $T_b$ ) for CFS buildings with varying numbers of stories is listed in Table 1. The current ASCE 7 height limit

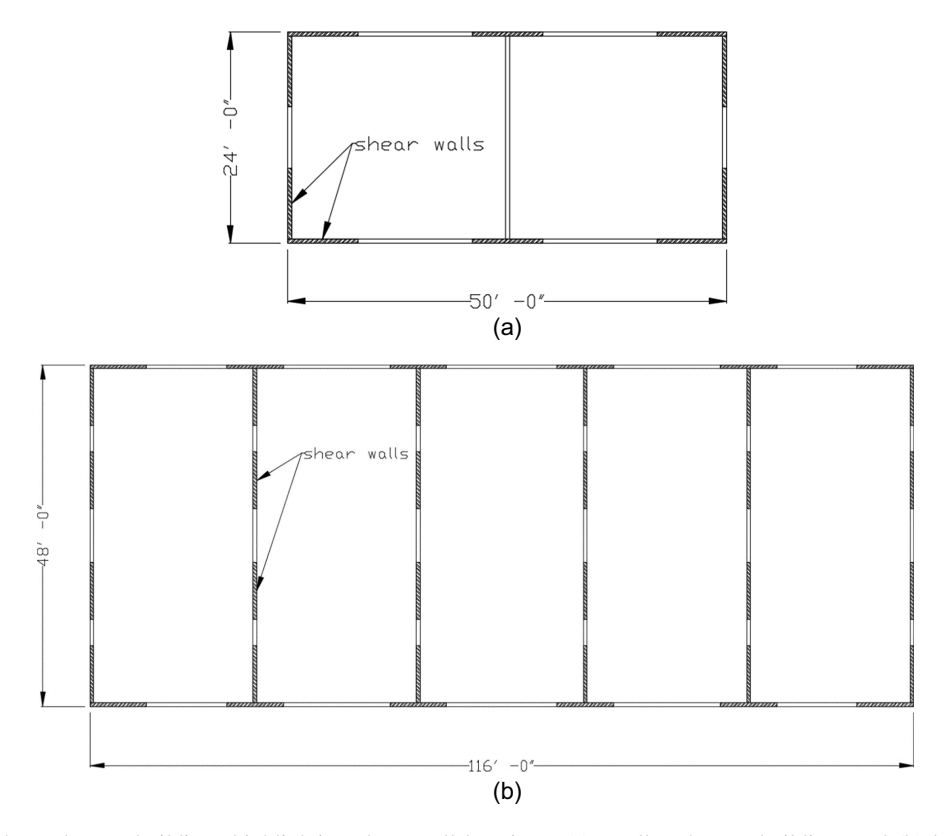


Fig. 2. Plan views of the archetype buildings highlighting shear wall locations: (a) small archetype building; and (b) large archetype building.

Table 1. Estimated periods of CFS buildings with different heights

Stories	H (ft)	H (m)	$T_b$ (s)
1	10	3.0	0.11
2	20	6.1	0.19
3	30	9.1	0.26
4	40	12.2	0.32
5	50	15.2	0.38
6	60	18.3	0.43

for CFS systems in high seismic zones is 19.8 m (65 ft), so assuming 3-m (~10-ft) story heights, the maximum number of stories for a typical CFS building is 6 (Table 1).

The base shear of a building can be determined using Eq. (9) assuming an importance factor of 1.0, where  $V_b$  is the base shear; n is the number of stories;  $m_w$  is the mass per floor [i.e., 240,000 lbf (1,068 kN) in the case of the large building];  $S_a$  is the pseudo spectral acceleration from the design spectrum, which is assumed to be  $S_a = S_{DS} = 1.0$  (consistent with a high-seismic site such as Irvine, California); and R is the seismic response modification coefficient for forces [6.5 in the case of WSP- or SS-CFS shear walls (ASCE 7-22)]. This study followed the ASCE 7 approach (but not exactly the ASCE 7 notation)

$$V_b = (nm_w)S_a/R \tag{9}$$

To initiate solving for the minimum required  $v_n$ , 100% utilization of the shear walls (SWs) employed in the building was assumed (this assumption was refined subsequently). Based on the plan dimensions of the building in the short direction, two perimeter wall lines were assumed to carry the demand in the small building, and six wall lines were assumed to carry demand in the large building. Hence, the length of shear walls was  $w_s \le 24 \times 2 = 48$  ft (14.6 m) for the small building and  $w_s \le 48 \times 6 = 288$  ft (87.8 m) for the large building. Assuming that 67% of  $w_s$  was utilized for shear walls in the short direction (67% is a convenient choice, made by the authors, which is consistent with statistics of typical CFS buildings) and solving for  $v_n$  using Eq. (10), the minimum required  $v_n$  for buildings with 1–6 stories is listed in Table 2

$$V_b = \gamma \varphi v_n w_s \tag{10}$$

where  $\gamma = \text{SWs}$  length-to-wall line length ratio;  $w_s = \text{summation of}$  shear wall lengths in the short direction;  $\varphi = \text{resistance factor } (0.60 \text{ in AISI S400-20})$ ; and  $v_n = \text{nominal shear strength per unit length.}$ 

For design, a WSP or SS shear wall from the AISI S400 tables should be chosen to satisfy the minimum required  $v_n$  for any building in these table. Assuming that all shear walls are 8 ft (2.44 m) wide and that q is the number of identical shear walls in the first story, and using the actual  $v_n$  for the chosen wall from the AISI S400-20 tables, the number of shear walls in the first story (q),

the capacity of a single shear wall  $(V_s)$ , and the utilization of shear walls  $(\alpha)$  can be determined from the following equations:

$$w_s \ge \frac{V_b}{\varphi v_n} \tag{11}$$

$$q = \text{ceiling}\left(\frac{w_s}{8}\right) \tag{12}$$

$$V_s = v_n \times 8 \text{ ft} \tag{13}$$

$$\alpha = V_b/q\varphi V_s \tag{14}$$

where  $\operatorname{ceiling}(X)$  rounds up X to the nearest integer;  $w_s$  is in feet;  $V_s$  and  $V_b$  are in pounds; and  $v_n$  is in pounds/foot.

Not all walls are controlled by strength. ASCE 7 provides an upper drift limit of 2.5%h. In the case of walls that are drift-controlled [i.e.,  $C_d\delta_{S400}(\alpha\varphi V_n) > 2.5\%h$ ], q and  $\alpha$  were recalculated after decreasing the wall utilization so that  $C_d\delta_{S400}(\alpha\varphi V_n) \leq 2.5\%h$  is met. The details of the large archetype buildings utilizing WSP and SS shear walls using AISI S400-20 and ASCE 7-22 are provided in Table 3.

There are multiple possible solutions for a given story height (Table 3), which reflects a variety of WSP or SS shear walls that may be employed successfully for a given demand. In each case, the selected capacity,  $v_n$ , aligns with a specific shear wall, including complete seismic detailing as provided in AISI S400. Each entry in the AISI S400 tables is based on previously conducted shear wall experiments. Using the database of experimental CFS shear wall tests compiled by Ayhan et al. (2018), one also can associate the actually experimental shear wall performance with any entry in the AISI S400 shear wall strength tables. Hence, the expected nonlinear shear-deformation response of any selected CFS WSP or SS shear wall is known and may be utilized directly in modeling.

To connect individual shear wall responses to the idealized building response, an equivalent nonlinear SDOF model was used. Hence, the mass  $(m_{\rm eq})$  and stiffness  $(k_{\rm eq})$  of a single -degree-of-freedom model representing an archetype building, employing any of the S400 tabulated SWs as the main SFRS, was calculated per the following (Chopra 2017):

$$m_{\rm eq} = \frac{\sum i^2}{n^2} m_w \tag{15}$$

$$k_{\rm eq} = \frac{k_w}{n} \tag{16}$$

where  $k_w$  = sum of shear walls stiffness  $(k_s)$  in a story; and i = story number (i.e.,  $\Sigma i^2 = 1^2 + 2^2 + 3^2$  for a three-story building). Using Eq. (16), the nonlinear shear-wall stiffness  $k_{\rm eq}$  determined from experimental data ( $V_{\rm exp}$  versus  $\delta_{\rm exp}$  curve) is scaled as follows:

**Table 2.** Minimum required  $v_n$  for buildings with different heights

		$V_b$ [18	of (kN)]	$\min v_n [plf (kN/m)]$	$\min v_n [plf (kN/m)]$	
Stories (n)	H [ft (m)]	$T_b$ (s)	Small building	Large building	for small building $(w_s = 67\% \times 48 \text{ ft})$	for large building $(w_s = 67\% \times 288 \text{ ft})$
1	10 (3.05)	0.112	6,154 (27.37)	36,923 (164.24)	319 (4.65)	319 (4.65)
2	20 (6.10)	0.189	12,308 (54.75)	73,846 (328.48)	638 (9.31)	638 (9.31)
3	30 (9.15)	0.256	18,462 (82.12)	110,769 (492.73)	957 (13.96)	957 (13.96)
4	40 (12.20)	0.318	24,615 (109.49)	147,692 (656.97)	1,276 (18.62)	1,276 (18.62)
5	50 (15.25)	0.376	30,769 (136.87)	184,615 (821.21)	1,595 (23.28)	1,595 (23.28)
6	60 (18.30)	0.431	36,923 (164.24)	221,538 (985.45)	1,914 (27.93)	1,914 (27.93)

Note: plf = pound per liner foot.

Table 3. Details of large archetype buildings employing WSP- and SS-CFS shear walls tabulated in AISI S400-20

Wall type	$v_n$ (lb/ft)	$v_n$ (kN/m)	n	$V_b$ (lbf)	$V_b$ (kN)	Drift ratio (%)	q	$\alpha$	$1/(\alpha\varphi)$	Dominant
WSP	780	11.4	2	73,846	328.5	1.53	25	0.79	2.1	Strength
WSP	890	13.0	2	73,846	328.5	1.53	25	0.69	2.4	Strength
WSP	700	10.2	2	73,846	328.5	1.53	25	0.88	1.9	Strength
WSP	915	13.4	2	73,846	328.5	1.53	25	0.67	2.5	Strength
WSP	825	12.0	2	73,846	328.5	1.53	25	0.75	2.2	Strength
WSP	940	13.7	2	73,846	328.5	1.53	25	0.65	2.6	Strength
WSP	990	14.4	3	110,769	492.7	3.03	28	0.83	2.0	Drift
WSP	1,235	18.0	3	110,769	492.7	2.64	26	0.72	2.3	Drift
WSP	1,230	18.0	3	110,769	492.7	2.64	26	0.72	2.3	Drift
WSP	1,330	19.4	4	147,692	657.0	4.5	35	0.66	2.5	Drift
WSP	1,545	22.5	4	147,692	657.0	4.5	35	0.57	2.9	Drift
WSP	1,410	20.6	4	147,692	657.0	4.5	35	0.62	2.7	Drift
WSP	1,775	25.9	5	184,615	821.2	6.85	43	0.5	3.3	Drift
WSP	1,760	25.7	5	184,615	821.2	6.85	43	0.51	3.3	Drift
WSP	1,850	27.0	5	184,615	821.2	6.85	43	0.48	3.5	Drift
WSP	2,190	32.0	6	221,538	985.5	9.42	51	0.41	4.1	Drift
WSP	2,060	30.1	6	221,538	985.5	9.69	52	0.43	3.9	Drift
WSP	2,350	34.3	6	221,538	985.5	9.42	51	0.39	4.3	Drift
WSP	2,310	33.7	6	221,538	985.5	9.42	51	0.39	4.3	Drift
WSP	3,080	44.9	6	221,538	985.5	9.42	51	0.29	5.7	Drift
SS	390	5.7	1	36,923	164.2	0.52	25	0.79	2.1	Strength
SS	647	9.4	2	73,846	328.5	1.53	25	0.95	1.8	Strength
SS	710	10.4	2	73,846	328.5	1.53	25	0.87	1.9	Strength
SS	778	11.4	2	73,846	328.5	1.53	25	0.79	2.1	Strength
SS	845	12.3	2	73,846	328.5	1.53	25	0.73	2.3	Strength
SS	910	13.3	2	73,846	328.5	1.53	25	0.68	2.5	Strength
SS	1,000	14.6	3	110,769	492.7	3.03	28	0.82	2.0	Drift
SS	1,085	15.8	3	110,769	492.7	3.03	28	0.76	2.2	Drift
SS	1,170	17.1	3	110,769	492.7	2.64	26	0.76	2.2	Drift
SS	1,015	14.8	3	110,769	492.7	3.03	28	0.81	2.1	Drift
SS	1,040	15.2	3	110,769	492.7	3.03	28	0.79	2.1	Drift
SS	1,070	15.6	3	110,769	492.7	3.03	28	0.77	2.2	Drift
SS	1,055	15.4	3	110,769	492.7	3.03	28	0.78	2.1	Drift
SS	1,170	17.1	3	110,769	492.7	2.64	26	0.76	2.2	Drift
SS	1,235	18.0	3	110,769	492.7	2.64	26	0.72	2.3	Drift
SS	1,355	19.8	4	147,692	657.0	4.5	35	0.65	2.6	Drift
SS	1,305	19.0	4	147,692	657.0	4.5	35	0.67	2.5	Drift
SS	1,505	22.0	4	147,692	657.0	4.5	35	0.58	2.9	Drift
SS	1,870	27.3	5	184,615	821.2	6.85	43	0.48	3.5	Drift
SS	2,085	30.4	6	221,538	985.5	9.69	52	0.43	3.9	Drift

$$V_{\rm eq} = \max(\Omega_o \alpha \varphi, 1) \times q V_{\rm exp} \times \left(\frac{8'}{b_{\rm exp}}\right)$$
 (17)

$$\delta_{\rm eq} = n\delta_{\rm exp} \tag{18}$$

where  $\Omega_o$  = system overstrength factor (which equals 3.0 for CFS shear walls according to ASCE 7-22);  $V_{\rm eq}$  = scaled experimental strength;  $V_{\rm exp}$  = nonscaled (measured) experimental strength;  $\delta_{\rm eq}$  = experimental deflection scaled to account for number of stories in the considered building;  $\delta_{\rm exp}$  = nonscaled (measured) experimental deflection; and  $8'/(b_{\rm exp})$  accounts for the difference between the experimental shear-wall's width  $b_{\rm exp}$  (feet) and the assumed width for identical shear walls in the studied archetype buildings [i.e., 8 ft (2.44 m)].

The system (i.e., the whole building) overstrength is accounted for in Eq. (17) by connecting it to the individual shear walls' overstrength. Shear wall designs already include some overstrength due to (1) utilization of shear walls  $(\alpha)$ , and (2) the resistance factor  $(\varphi)$ . Hence, an overstrength of  $1/(\alpha\varphi)$  is expected. In some cases,  $\alpha$  may be small enough to lead to an overstrength greater than the system overstrength  $\Omega_o$  (which equals 3.0). To account for such cases when  $1/(\alpha\varphi) > \Omega_o$  (i.e., to allow overstrength greater

than 3 if it comes directly from the design), the maximum of  $\Omega_o \alpha \varphi$  or 1.0 is used to define the system overstrength factor [the term max  $(\Omega_o \alpha \varphi, 1)$  in Eq. (17)]. The  $1/(\alpha \varphi)$  values for the investigated large archetype buildings are listed in Table 3.

The choice of the equivalent SDOF model for this study reflected the fact that the primary nonlinearity in the investigated system is that derived from the shear wall behavior. Regardless of whether flexible- or rigid-diaphragm assumptions are adopted, this fact is unchanged. The key differences between the two methods for the investigated cases are potentially the distribution of the force to the shear walls and the potential for additional demands due to torsion. The simple buildings that were studied here had nominal centers of mass and centers of stiffness coinciding, so no intentional eccentric was necessary. In addition, the way the shear walls were selected in the investigated buildings led to demands that coincided for flexible and rigid diaphragms. Thus, under the simplifying assumptions utilized in this study, an equivalent SDOF model was an appropriate choice.

The equivalent SDOF model was implemented in OpenSees to perform nonlinear time-history analyses of the archetype buildings. For each individual archetype building, an equivalent-energy Pinching4 (EEP4) model was fitted to the corresponding

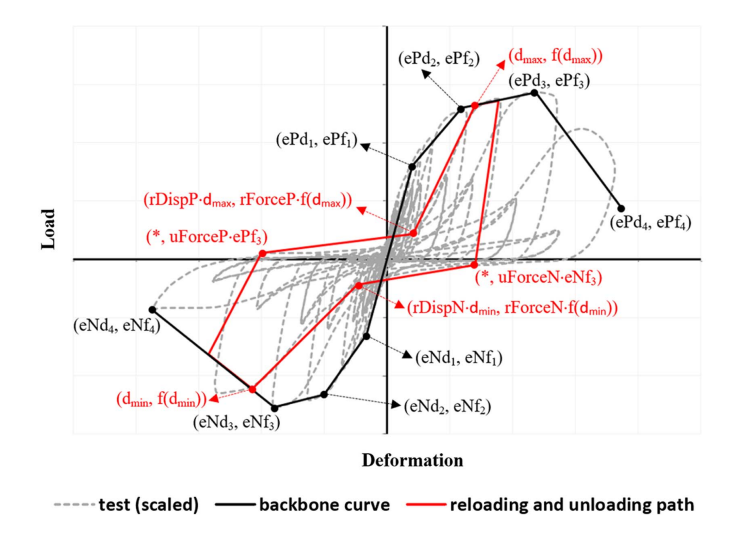


**Fig. 3.** Equivalent-energy Pinching4 fit to the scaled experimental response of Specimen 22A tested by Branston (2004).

experimental data scaled. This multilinear Pinching4 backbone curve utilized the peak scaled tested strength as an anchor point in both force and deformation, and used a two-part linear curve (prepeak and postpeak) with adjusted slopes to match the energy in the scaled experimental curve. A typical fit is shown in Fig. 3. The parameters used to define the Pinching4 material (PEER 2019) include ePf1-4, ePd1-4, eNf1-4, and eNd1-4 (floating point values defining force/deformation points on the positive or negative response envelope); rDispP, rForceP, rDispN, rForceN (floating point values defining the ratio of the deformation/force at which reloading occurs to the maximum or minimum historic deformation

demand); uForceP, uForceN (floating point values defining the ratio of strength developed upon unloading from negative or positive load to the maximum or minimum strength developed under monotonic loading); other parameters controlling the cyclic degradation model for unloading and reloading stiffness degradation as well as strength degradation; and the defining maximum energy dissipation under cyclic loading (Lowes et al. 2003).

To calibrate the Pinching4 model parameters based on the experimentally measured scaled response of a cyclically loaded shear wall, a multistage energy-based local optimization protocol was utilized to achieve two main objectives: (1) produce backbone curves, pinching behaviors, and degradation behaviors analogous to those obtained experimentally; and (2) minimize the error in the cumulative energy (cumulative absolute value of area under the force–displacement hysteretic curve).

A damping ratio of 5% was adopted, which is consistent with past analyses of CFS systems (Dubina 2008; Shamim and Rogers 2013; Leng et al. 2017; Kechidi et al. 2017).

Finally, to determine the design basis excitation for each model, the logarithmic mean of the FEMA P-695 far-field earthquakes suite (FEMA 2009) was scaled such that  $S_{DS}=1.0$ . With the approach taken, the uncertainty and variation in the stiffness and strength of CFS-framed shear walls were incorporated, as well as the uncertainty of the excitation. Thus, a sufficiently robust procedure for examining deflections was employed.

A schematic diagram of the employed OpenSees model is shown in Fig. 4. The overall lateral stiffness and strength of the CFS shear walls is accounted for using an equivalent simple Pinching4 zeroLength element (PEER 2019) joined to rigid truss elements which transfer the force to the boundary studs resisting tension and compression stresses (Fig. 4).

Because this study focused on deflection, the key outcome of analysis was the peak story drift. This peak story drift can be

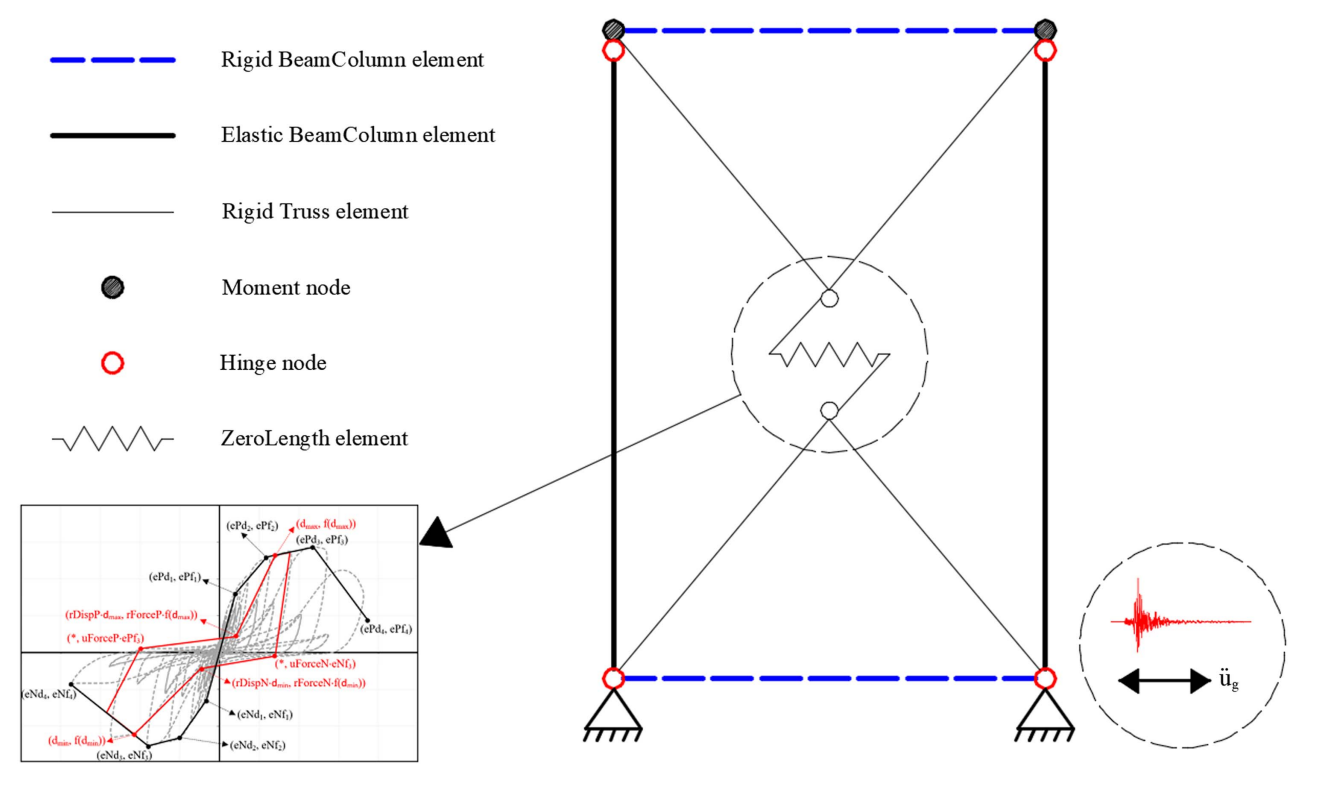


Fig. 4. OpenSees numerical model of an archetype building employing CFS shear walls.

determined from the numerically predicted peak deflection of the equivalent SDOF model as follows:

$$\delta_{sd}^{NL} = \delta_{eq}^{NL}/n \tag{19}$$

where  $\delta_{sd}^{NL}$  = peak numerical story drift (i.e., the peak drift of an individual shear wall); and  $\delta_{\rm eq}^{NL}$  = numerical peak nonlinear deflection of the considered building.

### **Parametric Study**

In this study, all shear walls in the database of cold-formed steel shear wall (CFSSW) experimental studies (Ayhan et al. 2018) obeying the detailing in AISI S400-20 were investigated. This covered a total of 118 shear walls across a wide range of key geometric and material parameters, including shear wall type, sheathing thickness, sheathing screw size, fastener spacing at panel edges, and hold-down employed. Each of these shear walls was modeled, incorporated into large and small buildings, and excited under the different 44 FEMA P-695 design-basis earthquakes (FEMA 2009), for a total of 5,192 (118 × 44) cases for the large building and 5,192 cases for the small building. Table 4 lists the key geometric and material parameters examined in the study and the number of large-building analyses associated with each parameter.

After the equivalent SDOF model was constructed, and because the force demand on a given wall was identical (Table 2), there is no noticeable difference between the findings for large buildings and small buildings, and hence only the results for large building are reported and discussed in the following sections.

### **Evaluation of AISI S400 Deflection Expression**

Employing the results of the 118 experimental studies considered, the AISI S400 deflection equation [Eq. (5)] was evaluated. For each case, the ratio of experimental deflection (determined using the

**Table 4.** Key parameters investigated in this study

Studied parameters	Parameter variations	No. of large-building analyses
Shear wall type	SS WSP	3,652 1,540
Sheathing thickness	7/16-in. (11.11-mm) WSP 0.018-in. (0.46-mm) SS 0.027-in. (0.68-mm) SS 0.03-in. (0.76-mm) SS 0.033-in. (0.84-mm) SS	1,540 660 836 1,276 880
Sheathing screw size	8 10	4,708 484
Fastener spacing at panel edges	6 in. (152.4 mm) 4 in. (101.6 mm) 3 in. (76.2 mm) 2 in. (50.8 mm)	2,640 1,012 264 1,276
Hold-down employed	S/HD10 <sup>a</sup> S/HD10S <sup>a</sup> S/HDU6 <sup>a</sup> Others	1,144 3,080 572 396

<sup>&</sup>lt;sup>a</sup>Hold-down response was not modeled separately, but is included in the overall response of the shear walls. Specifications of the hold-downs used are provided by Simpson Strong-Tie Company (2022).

backbone curve in the case of cyclic tests) to that calculated using the AISI S400 expression (i.e.,  $\delta_{\rm exp}/\delta_{\rm S400}$ ) was determined at four different force levels:  $0.4\phi V_n$ ,  $0.4V_n$ ,  $\phi V_n$ , and  $V_n$ , where  $\phi$  is the resistance factor (0.60 in AISI S400-20) and  $V_n$  is the nominal resistance ( $v_n = v_n$ /wall length in S400). In AISI test standards [e.g., AISI S907 (AISI 2013), related to cantilever diaphragm testing], it is common to use 40% of the ultimate load for an approximation of the elastic stiffness; this was explored by Leng et al. (2017) and shown to be conservative. This is based on the facts that initial accommodation (in the measured force–deformation response) usually is established and the response is relatively linear up to this force level, and that 40% of  $V_n$  is a reasonable approximation of service load levels.

Because the parameters of the AISI S400 deflection expression vary depending on wall type (AISI 2020), the results of each wall type (i.e., WSP or SS) were considered separately. Key statistics for  $\delta_{\rm exp}/\delta_{\rm S400}$  including mean, standard deviation, and coefficient of variation (COV) are listed in Tables 5 and 6 for WSP and SS cases, respectively.

It is clear that nonlinear static deflection predictions from AISI S400 are approximate. At design level with 100% utilization  $(\phi V_n = 0.6 V_n)$ , the S400 expression was conservative for both WSP and SS shear walls, although variation was large. At lower force levels, the WSP predictions were more consistent than the SS predictions. Variation in the predictions have multiple sources, but the experimental strength varied with respect to  $v_n$ , in addition to direct variation in the drift. Ultimately, the AISI S400 deflection expression can be judged by its coupling with  $C_d$  and its prediction of dynamic nonlinear drift, which is studied in the next section. However, further research on the assessment of AISI S400 deflection expression and the sources of its lack of predictive accuracy is recommended.

### **Evaluation of Actual and AISI S400 Deflection Amplification Factors**

As shown previously [Eq. (4)], the deflection amplification factor,  $C_d$ , equals the ratio of nonlinear deflection (i.e., in this study, the deflection determined by nonlinear time-history analysis) to elastic deflection. Employing the parametric study's results for the nonlinear dynamic response of 118 archetype buildings excited by the 44 FEMA earthquakes (i.e., 5,192 analyses), actual and AISI

**Table 5.** Key statistics of  $\delta_{\rm exp}/\delta_{\rm S400}$  for investigated 35 WSP cases at different force levels

Force level	Mean	Standard deviation	COV
$0.24V_n$	0.79	0.35	0.44
$0.4V_n$	0.78	0.24	0.31
$0.6V_n$	0.73	0.15	0.21
$V_n$	0.90	0.35	0.38

**Table 6.** Key statistics of  $\delta_{\rm exp}/\delta_{\rm S400}$  for investigated 83 SS cases at different force levels

Force level	Mean	Standard deviation	COV
$0.24V_n$	1.41	3.35	2.38
$0.4V_n$	1.06	2.05	1.94
$0.6V_n$	0.64	0.37	0.58
$V_n$	0.78	0.47	0.60

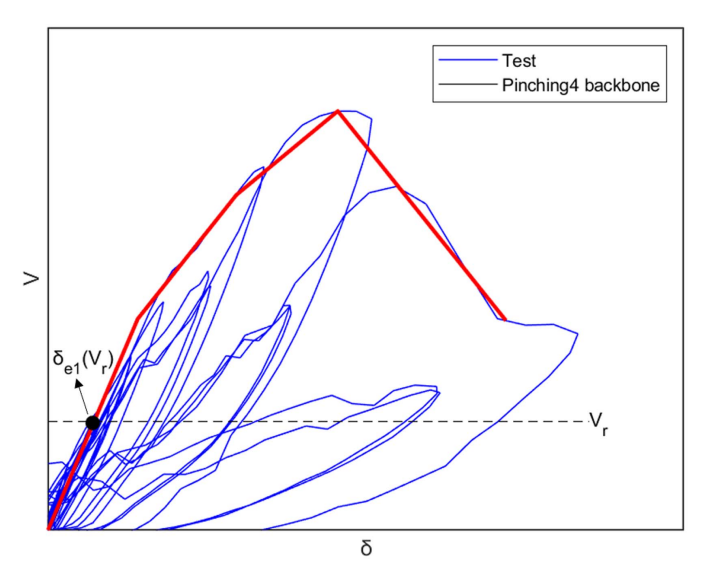


**Fig. 5.**  $\delta_{e1}(V_r)$  used to calculate  $C_{d1}$ .

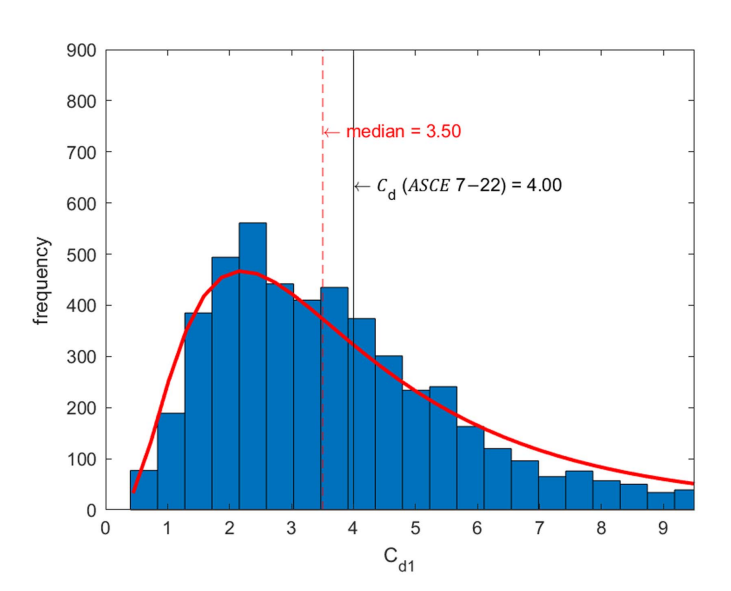


**Fig. 6.** Histogram of  $C_{d1}$  for all 5,192 cases considered in this study.

S400 deflection amplification factors (referred to in this paper as  $C_{d1}$  and  $C_{d2}$ , respectively) were investigated.

This section first, considers the actual elastic deflection (i.e., that calculated using the initial slope of the Pinching4 backbone curve determined based on experimental data) and uses it to calculate  $C_{d1}$ , and then compares it against  $C_d$  in current practice ( $C_{d2}$ ) that

employs the nonlinear S400 deflection expression to find elastic deflection. All elastic deflections utilized in this study for  $C_d$  calculations were determined at the required shear demand level (Table 3,  $V_b$ ).

### C<sub>d1</sub> (Actual C<sub>d</sub>, i.e., Employing the Initial Slope of the Experimental Pinching4 Backbone Curve)

This subsection determined the initial slope of the nonscaled Pinching4 backbone curve directly from the experimental results that were employed to find the elastic deflection at the required shear demand level of an individual shear wall,  $\delta^{e1}$  ( $V_r$ ) (Fig. 5). Hence,  $C_{d1}$  was calculated utilizing Eq. (20), where  $\delta^{NL}_{sd}$  is the numerically predicted peak nonlinear story drift determined per Eq. (19). Parameter  $C_{d1}$  can be considered to be the real  $C_d$  because it uses the actual (experimental) results to obtain both elastic and plastic deflections for the  $C_d$  calculations

$$C_{d1} = \frac{\delta_{sd}^{NL}}{\delta^{e1}(V_r)} \tag{20}$$

Fig. 6 shows a histogram of  $C_{d1}$  for the 5,192 cases considered in this study with a lognormal distribution superimposed, and Table 7 shows key statistics including mean, median, mode,  $\sigma$ , COV, and exceedance probability. The distribution of  $C_{d1}$  reasonably can be modeled with a lognormal distribution (with a median value of 3.5 and an exceedance probability of 41% based on raw data) (Fig. 6).

### C<sub>d2</sub> (Current Practice)

In current practice, the AISI S400 nonlinear deflection expression [Eq. (5)] is utilized to find elastic deflection for  $C_d$  (or  $\delta_{sd}^{NL}$ ) calculations. In current practice,  $C_d$  (i.e.,  $C_{d2}$ ) can be calculated using Eq. (21), for which  $\delta^{e2}(V_r)$  is plotted in Fig. 7

$$C_{d2} = \frac{\delta_{sd}^{NL}}{\delta^{e2}(V_r)} \tag{21}$$

Fig. 8 shows a histogram of  $C_{d2}$  for the studied 5,192 cases with the lognormal distribution superimposed, and Table 7 lists key statistics of  $C_{d2}$ . The distribution of  $C_{d2}$  can be well represented by a lognormal distribution (with a median of 2.19 and an exceedance probability of 15% based on raw data) (Fig. 8).

As mentioned in the section "Introduction," methods proposed for calculating  $C_d$  for other steel systems (Fahnestock et al. 2007; Kuşyılmaz and Topkaya 2015; Yakhchalian et al. 2020) depend on minimizing the difference between the mean value of  $C_d$  obtained from nonlinear numerical analyses of systems under design-level shaking and that calculated analytically. In those studies, the highest reported discrepancy between the mean of numerical and analytical deflection amplification factors was less than 8%. This is not the case for  $C_d$  of cold-formed steel systems in current practice

**Table 7.** Key statistics of different forms of  $C_d$  considered in this study

			Raw c	lata			Lognor	mal fit
Considered $C_d$	Mean	Median	Mode	$\sigma$	COV	$P_{Cd>4}$	Mean	$\sigma$
$C_{d1}$ (experimental elastic stiffness)	4.92	3.50	0.54	8.17	1.66	0.41	1.27	0.70
$C_{d2}$ (current practice)	2.62	2.19	1.17	2.32	0.89	0.15	0.74	0.67
$C_{d3}$ (S400 secant at $0.4V_r$ )	4.14	3.40	1.83	3.73	0.90	0.41	1.19	0.67
$C_{d4}$ (S400 elastic stiffness)	6.86	5.45	2.90	6.46	0.94	0.68	1.67	0.70

Note: Lognormal fit mean and  $\sigma$  = mean and standard deviation, respectively, of lognormal distribution superimposed on a histogram.

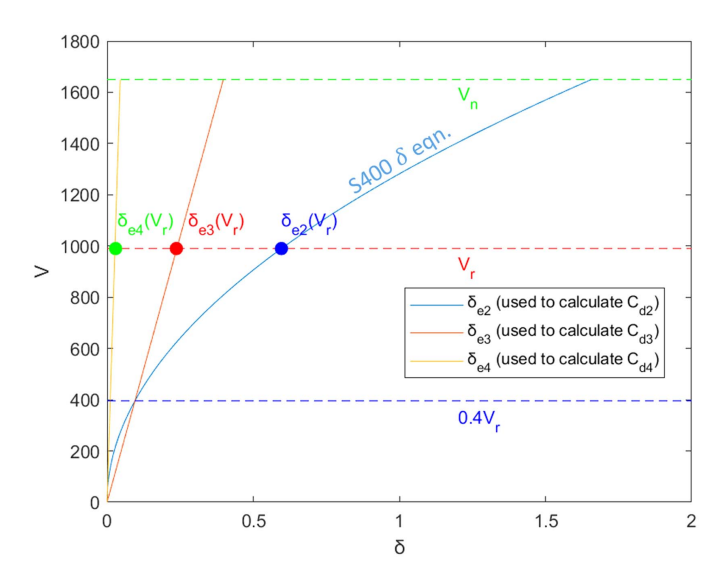


**Fig. 7.**  $\delta_{e2}(V_r)$ ,  $\delta_{e3}(V_r)$ , and  $\delta_{e4}(V_r)$  utilized to determine  $C_{d2}$ ,  $C_{d3}$ , and  $C_{d4}$ , respectively.

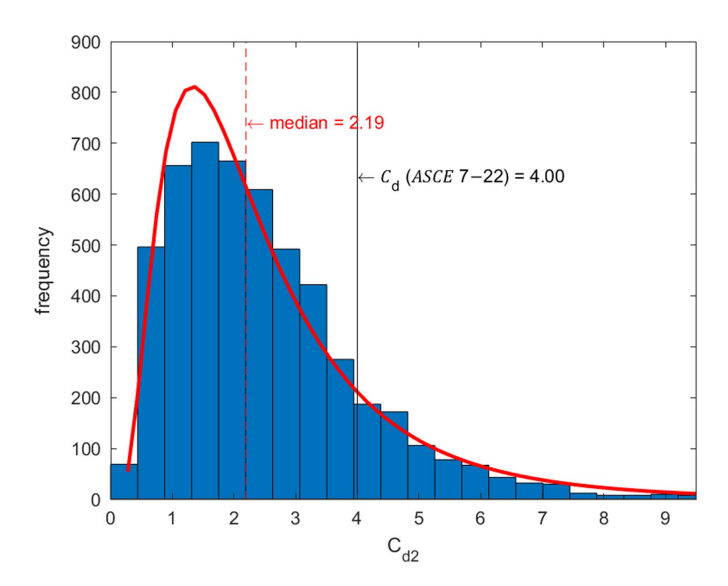


**Fig. 8.** Histogram of  $C_{d2}$  for the investigated 5,192 cases.

(i.e.,  $C_{d2}$ ); the  $C_d$  value for CFS systems per ASCE 7-22 is 1.53 times the mean value of  $C_{d2}$  (Table 7). This discrepancy indicates that the current practice for application of  $C_d$  may be overly conservative, and improved methods for calculating  $C_d$  (or  $\delta_{sd}^{NL}$ ) should be proposed for better accuracy [comparing the median value of  $C_{d2}$  with ASCE 7  $C_d$  leads to the same conclusion (Fig. 8)]. To this end, two linear analytical methods for finding elastic deflections delivering less-conservative  $C_d$ 's are suggested in the following section.

### Considered Linear Methods for Calculating Deflection Amplification Factor

This section explores two analytically linear approaches for finding the deflection to be amplified by  $C_d$  (or  $\delta_{sd}^{NL}$ ). Hence, two different versions of  $C_d$  (calculated depending on the two

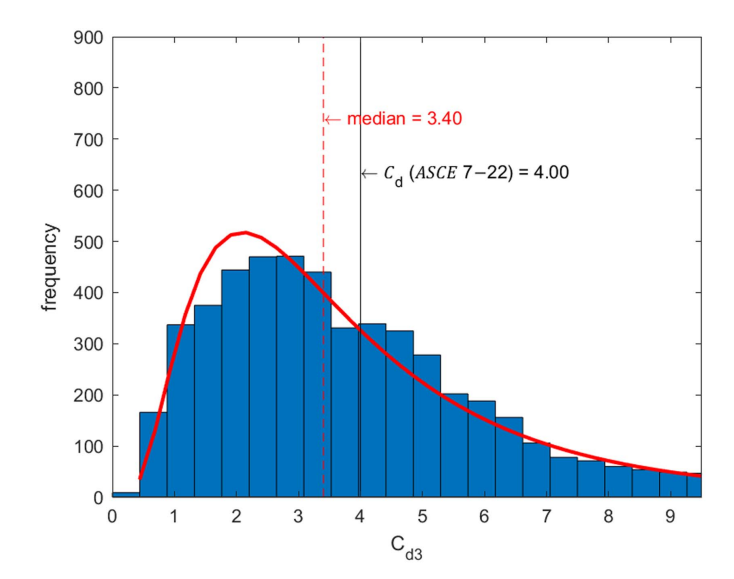


**Fig. 9.** Histogram of  $C_{d3}$  for the 5,192 analyses.

proposed elastic deflections) were considered:  $C_{d3}$ , determined based on the secant stiffness of S400 curve at  $0.4V_r$ , and  $C_{d4}$ , calculated using the elastic stiffness (slope at V=0) of the S400 deflection expression curve. As mentioned previously, both of these elastic deflections are calculated at the required shear demand level ( $V_r$ ).

# $C_{d3}$ (Employing the Secant Stiffness of S400 Curve at $0.4V_r$ )

In this subsection, a deflection amplification factor (referred to as  $C_{d3}$ ) is calculated depending on  $\delta^{e3}(V_r)$  [Eq. (22)], where  $\delta^{e3}(V_r)$  is the deflection at  $V_r$  on the secant line of the S400 curve at  $0.4V_r$  (Fig. 7)

$$C_{d3} = \frac{\delta_{sd}^{NL}}{\delta^{e3}(V_r)} \tag{22}$$

Fig. 9 shows a histogram of  $C_{d3}$  for all 5,192 cases considered in this study with the fitting lognormal distribution, and Table 7 presents key statistics of  $C_{d3}$ . The distribution of  $C_{d3}$  can be well represented with a lognormal distribution (with a median value of 3.40 and an exceedance probability of 41%) (Fig. 9). The statistics of  $C_{d3}$  are promising (Table 7), with mean values much closer to those recommended than are the other forms of  $C_{d}$  considered in this study; a COV (determined based on raw data) of 0.9; and, more importantly, the same exceedance of the actual  $C_{d}$  (i.e.,  $C_{d1}$ ).

### C<sub>d4</sub> (Utilizing the Elastic Stiffness of S400 Curve)

The fourth method for determining deflection amplification factor (referred to as  $C_{d4}$ ) utilizes the initial stiffness of the S400 expression per Eq. (23) and  $\delta^{e4}(V_r)$  (Fig. 7), where  $\delta^{e4}(V_r)$  is the deflection at  $V_r$  on the initial stiffness line of S400 curve (Fig. 7)

$$C_{d4} = \frac{\delta_{sd}^{NL}}{\delta^{e4}(V_r)} \tag{23}$$

A histogram of  $C_{d4}$  for the 5,192 studied cases (118 archetype buildings excited by the 44 FEMA earthquakes) with the lognormal distribution superimposed is illustrated in Fig. 10, and key statistics are listed in Table 7. The distribution of  $C_{d4}$  could be modeled with

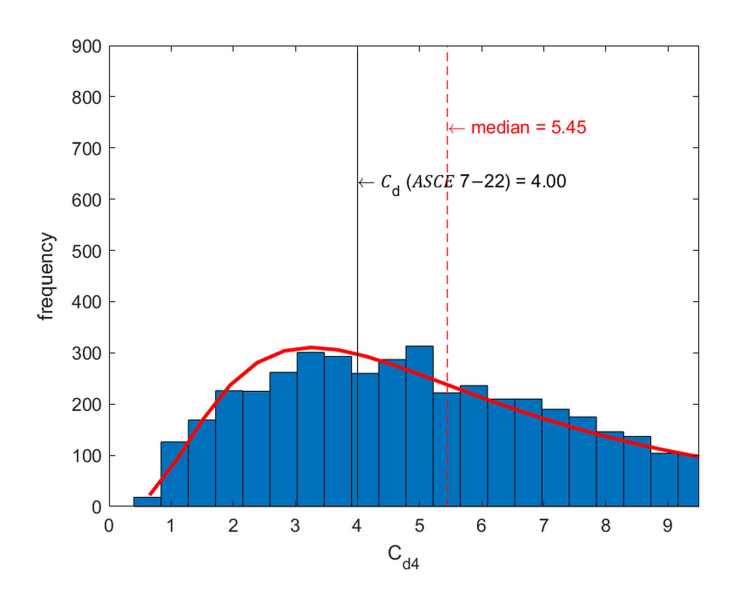


**Fig. 10.** Histogram of  $C_{d4}$  for the considered 5,192 cases.

a lognormal distribution (with a median of 5.45 and an exceedance probability of 68% based on raw data) (Fig. 10). However, the columns of the  $C_{d4}$  histogram do not clearly form the usual bell shape of normal distributions; there is a much steeper superimposed lognormal distribution of  $C_{d4}$  than those of other investigated forms of  $C_d$ . Moreover, the mean of  $C_{d4}$  is much higher than that recommended in current practice (i.e., 1.71 times the ASCE 7  $C_d$ ). Therefore, it can be concluded that the initial elastic stiffness is not a good metric to use for determining elastic deflection of CFS shear walls. This is not surprising, because, unlike other steel systems that employ the calculated initial elastic stiffness, a great proportion of connection deformation in CFS systems is not incorporated fully into the initial stiffness expression.

### Discussion of $C_{d3}$

As shown previously,  $C_{d3}$  offers the most reasonable statistics among the forms of  $C_d$  studied. It can be represented by a lognormal distribution with a mean of 4.14 and a COV of 0.90 (Table 7). In addition to utilizing a straightforward linear method to determine elastic deflection, instead of the nonlinear equation adopted in AISI S400,  $C_{d3}$  provides less-conservative estimations for  $C_d$  than the overly conservative  $C_d$  in current practice, with a mean value only 3.50% higher than the ASCE 7 recommended value, and with an exceedance almost the same as that of the actual results (Table 7).

To investigate the full source of variation in  $C_{d3}$ , the effects of key parameters on the accuracy of  $C_{d3}$  predictions were studied (Fig. 11). The key parameters considered included wall strength, test-to-AISI peak strength ratio, number of building stories, and earthquake (EQ) record. It is clear that WSP cases had much less variance than SS cases (Fig. 11). The worst predictions were those for the lowest-strength SS shear walls and single-story buildings. EQ sensitivity also was present [Fig. 11(h)]. Nevertheless, these detected variances, which were expected given the variation across EQs and the variation across shear wall responses included in the study, did not affect the overall accuracy of  $C_{d3}$  (Table 7).

### **Recommendations for AISI S400**

Based on the discussion in the previous section, it is recommended to use  $\delta_{e3}$  as the elastic deflection for the plastic deflection

analytical calculations in lieu of the current nonlinear deflection expression in AISI S400. Parameter  $\delta_{e3}$  is calculated using the following linear equation (noting that the AISI S400 expression is linearized at  $v=0.4v_r\cong0.4\phi v_n=0.24v_n$ ):

$$\delta^{e3} = \left[ \frac{2h^3}{3EA_c b} + \omega_1 \omega_2 \frac{h}{\rho G t_{\text{sheathing}}} + \omega_1^{5/4} \omega_2 \omega_3 \omega_4 \frac{0.4 \varphi v_n}{\beta^2} + \frac{h}{0.4 \varphi v_n b} \delta_{v@0.4 \varphi v_n} \right] \cdot v$$
(24)

where  $\delta_{v@0.4\varphi v_n}$  = vertical deformation of anchorage or attachment at  $0.4\varphi v_n$ . The stiffness (k) is the inverse of the bracketed term of Eq. (24)

$$k = \left[ \frac{2h^3}{3EA_cb} + \omega_1\omega_2 \frac{h}{\rho Gt_{\text{sheathing}}} + \omega_1^{5/4}\omega_2\omega_3\omega_4 \frac{0.4\varphi v_n}{\beta^2} + \frac{h}{0.4\varphi v_n b} \delta_{v@0.4\varphi v_n} \right]^{-1}$$
(25)

The nonlinear deflection for buildings framed with CFS shear walls can be calculated analytically utilizing the following expression:

$$\delta^{NL} = C_d k^{-1} v_r \tag{26}$$

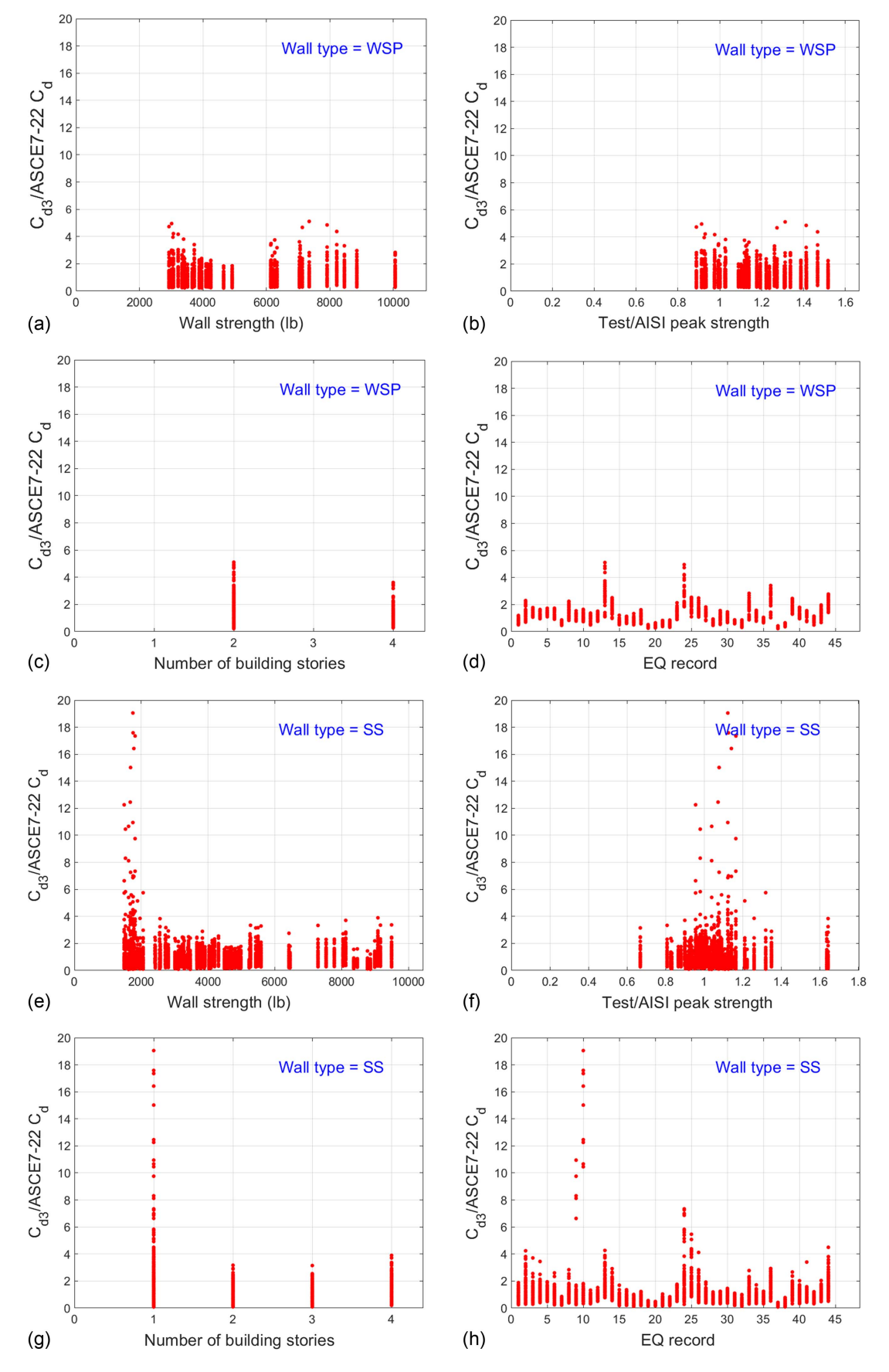
The parameters in the preceding equations are defined in detail in AISI S400-20 and in the Appendix to this paper. The value of v should not exceed  $\varphi v_n$  per AISI S400; the  $C_d$  value for CFS shear walls (i.e., 4.0) is given in ASCE 7-22. Linearization of the deflection expression is more consistent with the application of ASCE 7 to higher risk categories in which the importance factor,  $I_e$ , is greater than 1.0, because the demand force is increased by  $I_e$  and the drift is decreased by the same  $I_e$ .

Table 8 presents the peak nonlinear deflections calculated using the current AISI S400 expression, determined numerically based on experimental data, and calculated employing the proposed expression, for a CFS-SW with wood structural panel sheathing and for a CFS-SW with steel sheet sheathing. It is clear that the discrepancy between the current-practice estimate for peak deflection and that determined numerically based on experimental data is great (Table 8). This is not the case for the proposed equation, for which the discrepancy is much less.

### **Summary and Conclusions**

This study conducted a thorough numerical parametric investigation of the deflection amplification factor for 118 archetype buildings, employing cold-formed steel-framed shear walls and excited by 44 design-basis earthquakes, using nonlinear single-degree-of-freedom models constructed in OpenSees. Two types of cold-formed steel shear walls were taken into consideration: shear walls with wood structural panels, and shear walls with steel sheet sheathing. Exploiting available test data for the 118 shear walls investigated, in addition to the generated numerical results of the time-history analysis for the 5,192 cases (118 archetype building × 44 earthquakes), the AISI S400 deflection expression was assessed, and different methods for calculating deflection amplification (including the actual method, the AISI S400-20 method, and two proposed analytical methods) were investigated thoroughly.

Evaluation of the approach followed in current practice (AISI S400-20) for determining deflection amplification, based on the data from 5,192 numerical analyses, found a great discrepancy (35%) with the deflection amplification factor recommended by



**Fig. 11.** Effect of key parameters on the accuracy of  $C_{d3}$  estimations (separated by wall type).

**Table 8.** Peak nonlinear deflections, calculated using current AISI S400 expression, determined numerically based on experimental data, and calculated employing proposed expression for CFS-SWs

		Deflection (in.	)
Sheathing used	Based on tests	Current practice	Proposed expression
Wood structural panel <sup>a</sup> Steel sheet <sup>b</sup>	1.99 0.69	3.35 2.58	2.22 1.55

Note: Data of Test 2 in Liu et al. (2012) were used for the wood structural panel example, and the data of Test 11C-a in Balh and Rogers (2010) were used for the steel sheet example.

<sup>a</sup>Shear wall with 7/16-in. OSB wood structural panel sheathing; 6-in. fastener spacing at panel edges; and 54-mi designation thickness of stud, track, and stud blocking.

<sup>b</sup>Shear wall, with 0.027-in. steel sheet sheathing; 4-in. fastener spacing at panel edges; and 43-mi designation thickness of stud, track, and stud blocking.

ASCE 7. This considerable discrepancy indicates that the deflection prediction utilized in current practice may be overly conservative, and alternatives are worth considering.

Two linear methods for determining deflection amplification were considered. Both methods depend on linearizing the AISI S400-20 nonlinear deflection equation. One of the suggested methods uses the elastic stiffness of the AISI S400-20 equation, and the other employs the secant stiffness at 40% of the required shear demand.

The method utilizing the elastic stiffness delivered inaccurate predictions for deflection amplification, with a mean 70% higher than the deflection amplification factor adopted by ASCE 7. This was not unexpected, because, unlike some other steel structural systems that depend on initial elastic stiffness, the relatively high deformation of connections in cold-formed steel systems is not completely taken into account by the initial stiffness equation.

On the other hand, the second method employing the secant stiffness at 40% of the required shear demand provided the most acceptable statistics among the methods investigated, with a mean value of the predicted deflection amplification factor only 3.5% greater than that of ASCE 7, and with an exceedance probability matching actual and experimental data.

Therefore, it is recommended that a modified version of the AISI S400-20 equation linearized based on the secant stiffness at 40% of the required shear demand should be used to determine the elastic deflections used for plastic deflection analytical predictions, instead of the highly conservative AISI S400-20 nonlinear deflection expression employed in current practice.

## Appendix. Definitions of Coefficients in AISI S400 (AISI 2020) Deflection Equation

Coefficients in the AISI S400 (AISI 2020) deflection equation are defined as follows:

For shear walls sheathed with wood structural panels:

 $A_c = \text{gross cross-sectional area of chord member [in.}^2 \text{ (mm}^2)];$ 

b = length of the shear wall [in. (mm)];

E = modulus of elasticity of steel [29,500,000 psi (203,000 MPa)];

 $G = \text{shear modulus of sheathing material [lb/in.}^2 (MPa)];$ 

h = wall height [in. (mm)];

s = maximum fastener spacing at panel edges [in. (mm)];

 $t_{\text{sheathing}} = \text{nominal panel thickness [in. (mm)]};$ 

 $t_{\text{stud}} = \text{stud designation thickness [in. (mm)]};$ 

V = total lateral load applied to the shear wall [lb (N)];

v = V/b = shear demand [lb/in. (N/mm)];

 $\beta$  = 67.5 for plywood other than Canadian softwood plywood (CSP), 55 for oriented strand board (OSB) and CSP in US Customary Units (lb/in.<sup>1.5</sup>), 2.35 for plywood other than CSP, and 1.91 for OSB and CSP in SI units (N/mm<sup>1.5</sup>);

 $\delta$  = calculated deflection [in (mm)];

 $\delta_v$  = vertical deformation of anchorage or attachment at the load level specified [in (mm)];

 $\rho=1.85$  for plywood other than CSP, and 1.05 for OSB and CSP:

 $\omega_1 = s/6$  (for s in in.) or s/152.4 (for s in mm);

 $\omega_2 = 0.033/t_{\text{stud}}$  (for  $t_{\text{stud}}$  in in.) or  $0.838/t_{\text{stud}}$  (for  $t_{\text{stud}}$  in mm);

 $\omega_3 = \sqrt{(h/b)/2}$ ; and

 $\omega_4 = 1$  for wood structural panel sheathing.

For shear walls with steel sheet sheathing:

The definitions of  $A_c$ , b, E, G, h, s,  $t_{\rm sheathing}$ ,  $t_{\rm stud}$ , v, V,  $\delta$ ,  $\delta_v$ ,  $\omega_1$ ,  $\omega_2$ , and  $\omega_3$  are the same as those for shear walls with wood structural panels.

 $\beta = 29.12 \times (t_{\text{sheatting}}/0.018)$  (for  $t_{\text{sheathing}}$  in in.) (lb/in.<sup>1.5</sup>) or  $1.01 \times (t_{\text{sheathing}}/0.457)$  (for  $t_{\text{sheathing}}$  in mm) (N/mm<sup>1.5</sup>) for steel sheet:

 $\rho = 0.075 \times (t_{\rm sheathing}/0.018)$  (for  $t_{\rm sheathing}$  in in.) or  $0.075 \times (t_{\rm sheathing}/0.457)$  (for  $t_{\rm sheathing}$  in mm) for steel sheet; and

 $\omega_4 = \sqrt{33/Fy}$  (for  $F_y$  in ksi) or  $\sqrt{227.5/Fy}$  (for  $F_y$  in MPa) for steel sheet.

### **Data Availability Statement**

Some or all data, models, or code that support the findings of this study are available from the corresponding author upon reasonable request.

### **Acknowledgments**

This work is funded by the American Iron and Steel Institute (AISI) and the Steel Framing Industry Association (SFIA). The work also is partially funded by the National Science Foundation under Grant Nos. 1663348 and 1663569 as a part of the research project "Seismic Resiliency of Repetitively Framed Mid-Rise Cold-Formed Steel Building (CFS-NHERI)." The numerical work conducted herein was assisted by Zhidong Zhang, Astrid Fischer, Kara Peterman, Tara Hutchinson, and the whole CFS-NHERI team; the authors express gratitude for their great help.

### References

AISI (American Iron and Steel Institute). 2013. *Test standard for cantilever test method for cold-formed steel diaphragms*. AISI S907-13. Washington, DC: AISI.

AISI (American Iron and Steel Institute). 2020. North American standard for seismic design of cold-formed steel structural systems. AISI S400. Washington, DC: AISI.

ASCE. 2022. Minimum design loads and associated criteria for buildings and other structures. ASCE/SEI 7-22. Reston, VA: ASCE.

ATC. 1995. Structural response modification factors. Rep. No. ATC 19. Redwood City, CA: Applied Technology Council.

Ayhan, D., S. Baer, Z. Zhang, C. A. Rogers, and B. W. Schafer. 2018. "Cold-formed steel framed shear wall database." In *Proc., Int. Specialty Conf. on Cold-Formed Steel Structures*. Rolla, MO: Missouri Univ. of Science and Technology.

- Balh, N., and C. A. Rogers. 2010. "Development of seismic design provisions for steel sheathed shear walls." Master's thesis, Dept. of Civil Engineering, McGill Univ.
- Branston, A. E. 2004. "Development of a design methodology for steel frame/wood panel shear walls." M.Eng. thesis, Dept. of Civil Engineering and Applied Mechanics, McGill Univ.
- Chopra, K. A. 2017. Dynamics of structures: Theory and applications to earthquake engineering. 5th ed. Hoboken, NJ: Pearson.
- Dubina, D. 2008. "Behavior and performance of cold-formed steel-framed houses under seismic action." J. Constr. Steel Res. 64 (7–8): 896–913. https://doi.org/10.1016/j.jcsr.2008.01.029.
- Fahnestock, L. A., R. Sause, and J. M. Ricles. 2007. "Seismic response and performance of buckling-restrained braced frames." J. Struct. Eng. 133 (9): 1195–1204. https://doi.org/10.1061/(ASCE)0733-9445(2007) 133:9(1195).
- FEMA. 2009. Quantification of building seismic performance factors. FEMA P-695. Washington, DC: FEMA.
- Gogus, A., and J. W. Wallace. 2015. "Seismic safety evaluation of reinforced concrete walls through FEMA P695 methodology." *J. Struct. Eng.* 141 (10): 04015002. https://doi.org/10.1061/(ASCE)ST.1943 -541X.0001221.
- Hsiao, P. C., D. E. Lehman, and C. W. Roeder. 2013. "Evaluation of the response modification coefficient and collapse potential of special concentrically braced frames." *Earthquake Eng. Struct. Dyn.* 42 (10): 1547–1564. https://doi.org/10.1002/eqe.2286.
- Kechidi, S., N. Bourahla, and J. M. Castro. 2017. "Seismic design procedure for cold-formed steel sheathed shear wall frames: Proposal and evaluation." *J. Constr. Steel Res.* 128 (Jan): 219–232. https://doi.org/10.1016/j.jcsr.2016.08.018.
- Kurban, C. O., and C. Topkaya. 2009. "A numerical study on response modification, overstrength, and displacement amplification factors for steel plate shear wall systems." *Earthquake Eng. Struct. Dyn.* 38 (4): 497–516. https://doi.org/10.1002/eqe.866.
- Kuşyılmaz, A., and C. Topkaya. 2015. "Displacement amplification factors for steel eccentrically braced frames." *Earthquake Eng. Struct. Dyn.* 44 (2): 167–184. https://doi.org/10.1002/eqe.2463.
- Kuşyılmaz, A., and C. Topkaya. 2016. "Evaluation of seismic response factors for eccentrically braced frames using FEMA P695 methodology." *Earthquake Spectra* 32 (1): 303–321. https://doi.org/10.1193/071014 EQS097M.
- Leng, J., K. D. Peterman, G. Bian, S. G. Buonopane, and B. W. Schafer. 2017. "Modeling seismic response of a full-scale cold-formed steel-framed building." *Eng. Struct.* 153 (Dec): 146–165. https://doi.org/10.1016/j.engstruct.2017.10.008.

- Liu, P., K. D. Peterman, and B. W. Schafer. 2012. Test report on cold-formed steel shear walls. Research Rep. No. CFS-NEES-RR03. Baltimore: Johns Hopkins Univ.
- Lowes, L. N., N. Mitra, and A. Altoontash. 2003. A beam-column joint model for simulating the earthquake response of reinforced concrete frames. PEER Rep. No. 2003/10. Berkeley: Univ. of California.
- Madsen, R. L., N. Nakata, and B. W. Schafer. 2011. CFS-NEES building structural design narrative. CFS-NEES RR01. Baltimore: Johns Hopkins Univ.
- Mohammadi, M., and B. Kordbagh. 2018. "Quantifying panel zone effect on deflection amplification factor." Struct. Des. Tall Special Build. 27 (5): e1446. https://doi.org/10.1002/tal.1446.
- Samimifar, M., A. V. Oskouei, and F. R. Rofooei. 2015. "Deflection amplification factor for estimating seismic lateral deformations of RC frames." *Earthquake Eng. Eng. Vibr.* 14 (2): 373–384. https://doi.org /10.1007/s11803-015-0029-y.
- Schafer, B. W., et al. 2016. "Seismic response and engineering of cold-formed steel framed buildings." *Structures* 8 (2): 197–212. https://doi.org/10.1016/j.istruc.2016.05.009.
- Şeker, O., B. Akbas, J. Shen, and A. Z. Ozturk. 2014. "Evaluation of deflection amplification factor in steel moment-resisting frames." *Struct. Des. Tall Special Build*. 23 (12): 897–928. https://doi.org/10 .1002/tal.1090.
- Shamim, I., and C. A. Rogers. 2013. "Steel sheathed/CFS framed shear walls under dynamic loading: Numerical modelling and calibration." *Thin-Walled Struct.* 71 (Oct): 57–71. https://doi.org/10.1016/j.tws.2013.05.007.
- Simpson Strong-Tie Company. 2022. "S/HDU Holdown." Accessed December 15, 2022. https://www.strongtie.com/holdownsandtensionties \_coldformedsteelconstruction/s.hdu\_holdown/p/s.hdu.
- Singh, A., T. C. Hutchinson, S. Torabian, B. W. Schafer, K. D. Peterman, L. Padgett, and H. Jones. 2022. "Structural design narrative of the CFS-NHERI 10-story test building for multi-dimensional shake table testing." CFSRC Colloquium 2022. Accessed October 17, 2022. http://jhir.library.jhu.edu/handle/1774.2/67720.
- Uang, C.-M., and A. Maarouf. 1994. "Deflection amplification factor for seismic design provisions." J. Struct. Eng. 120 (8): 2423–2436. https:// doi.org/10.1061/(ASCE)0733-9445(1994)120:8(2423).
- Yakhchalian, M., N. Asgarkhani, and M. Yakhchalian. 2020. "Evaluation of deflection amplification factor for steel buckling restrained braced frames." J. Build. Eng. 30 (Jul): 101228. https://doi.org/10.1016/j.jobe .2020.101228.